




Employing *in vitro* metabolism to guide design of F-labelled PET probes of novel α -synuclein binding bifunctional compounds

Chukwunonso K. Nwabufu, Omozojie P. Aigbogun, Kevin J.H Allen, Madeline N. Owens, Jeremy S. Lee, Christopher P. Phenix & Ed S. Krol


To cite this article: Chukwunonso K. Nwabufu, Omozojie P. Aigbogun, Kevin J.H Allen, Madeline N. Owens, Jeremy S. Lee, Christopher P. Phenix & Ed S. Krol (2021) Employing *in vitro* metabolism to guide design of F-labelled PET probes of novel α -synuclein binding bifunctional compounds, *Xenobiotica*, 51:8, 885-900, DOI: [10.1080/00498254.2021.1943566](https://doi.org/10.1080/00498254.2021.1943566)


To link to this article: <https://doi.org/10.1080/00498254.2021.1943566>

 View supplementary material [↗](#)

 Published online: 30 Jun 2021.

 Submit your article to this journal [↗](#)

 Article views: 178

 View related articles [↗](#)

 View Crossmark data [↗](#)

RESEARCH ARTICLE



Employing *in vitro* metabolism to guide design of F-labelled PET probes of novel α -synuclein binding bifunctional compounds

Chukwunonso K. Nwabufo^{a*}, Omozogie P. Aigbogun^{b*}, Kevin J.H Allen^a, Madeline N. Owens^c, Jeremy S. Lee^c, Christopher P. Phenix^b and Ed S. Krol^a

^aDrug Discovery and Development Research Group, College of Pharmacy and Nutrition, University of Saskatchewan, Saskatoon, Canada; ^bDepartment of Chemistry, University of Saskatchewan, Saskatoon, Canada; ^cDepartment of Biochemistry, Microbiology and Immunology, University of Saskatchewan, Saskatoon, Canada

ABSTRACT

1. A challenge in the development of novel ¹⁸F-labelled positron emission tomography (PET) imaging probes is identification of metabolically stable sites to incorporate the ¹⁸F radioisotope. Metabolic loss of ¹⁸F from PET probes *in vivo* can lead to misleading biodistribution data as displaced ¹⁸F can accumulate in various tissues.
2. In this study we report on *in vitro* hepatic microsomal metabolism of novel caffeine containing bifunctional compounds (C₈-6-I, C₈-6-N, C₈-6-C₈) that can prevent *in vitro* aggregation of α -synuclein, which is associated with the pathophysiology of Parkinson's disease. The metabolic profile obtained guided us to synthesize stable isotope ¹⁹F-labelled analogues in which the fluorine was introduced at the metabolically stable N7 of the caffeine moiety.
3. An *in vitro* hepatic microsomal metabolism study of the ¹⁹F-labelled analogues resulted in similar metabolites to the unlabelled compounds and demonstrated that the fluorine was metabolically stable, suggesting that these analogues are appropriate PET imaging probes. This straightforward *in vitro* strategy is valuable for avoiding costly stability failures when designing radiolabelled compounds for PET imaging.

ARTICLE HISTORY

Received 3 May 2021
Revised 11 June 2021
Accepted 11 June 2021



KEYWORDS

Microsomal metabolism; Positron Emission Tomography; Imaging probe design; alpha-synuclein; Parkinson's disease


Introduction

Parkinson's disease is a neurodegenerative disorder that is characterized by the misfolding and aggregation of α -synuclein into fibrils, and the subsequent inclusion of the fibrils into cytoplasmic bodies known as Lewy bodies (Forno 1996; Samii et al. 2004; Davie 2008; Uversky 2008). In addition to the challenges associated with the accurate diagnosis of Parkinson's disease (Rajput et al. 1991; Hughes et al. 1992; Litvan et al. 1998; Hughes et al. 2001; Schrag et al. 2002; Tolosa et al. 2009; Rizzo et al. 2016), there is currently no cure for Parkinson's disease. Therefore, the development of disease-modifying drugs and differential diagnostic agents is a major focus of research in Parkinson's disease. Given its role in the pathophysiology of Parkinson's disease, α -synuclein is considered a druggable target for the development of disease-modifying drugs and differential diagnostic probes for Parkinson's disease. Our laboratory has been developing novel compounds that can interact with α -synuclein with the goal of preventing α -synuclein aggregation and the pathological pathway that leads to Parkinson's. Previous studies suggest that caffeine, nicotine, metformin, and 1-aminoindan may be neuroprotective (Ross and Petrovitch 2001; Bar Am

et al. 2004; Quik 2004; Bar-Am et al. 2010; Chau et al. 2010; Prediger 2010; Dimpfel and Hoffmann 2011; Postuma et al. 2012; Quik et al. 2012; Wahlqvist et al. 2012; Patil et al. 2014). Recently, we confirmed that caffeine, nicotine, metformin, and 1-aminoindan exert their neuroprotective effects by binding to and altering the conformation of α -synuclein (Kakish et al. 2015). To improve the efficacy of these compounds, we synthesized novel bifunctional compounds from a caffeine scaffold attached to 1-aminoindan (C₈-6-I), nicotine (C₈-6-N), and caffeine (C₈-6-C₈) (Figure 1) and determined their ability to bind to α -synuclein and prevent α -synuclein mediated toxicity in a yeast model of Parkinson's disease (Kakish et al. 2016). Our results from the study led us to conclude that C₈-6-I and C₈-6-N were the most promising candidates for preventing α -synuclein mediated toxicity in a yeast model of Parkinson's disease. Although C₈-6-C₈ did not show any therapeutic potential, it displayed the strongest binding to α -synuclein. In order to better understand the biodistribution of C₈-6-I, C₈-6-N and C₈-6-C₈ *in vivo*, we are developing methods to label the bifunctional compounds with ¹⁸F to use in positron emission tomography (PET) imaging studies.

CONTACT Ed S. Krol  ed.krol@usask.ca  Drug Discovery and Development Research Group, College of Pharmacy and Nutrition, University of Saskatchewan, Saskatoon, Canada

*These authors contributed equally to the work.

 Supplemental data for this article can be accessed [here](#).

© 2021 Informa UK Limited, trading as Taylor & Francis Group

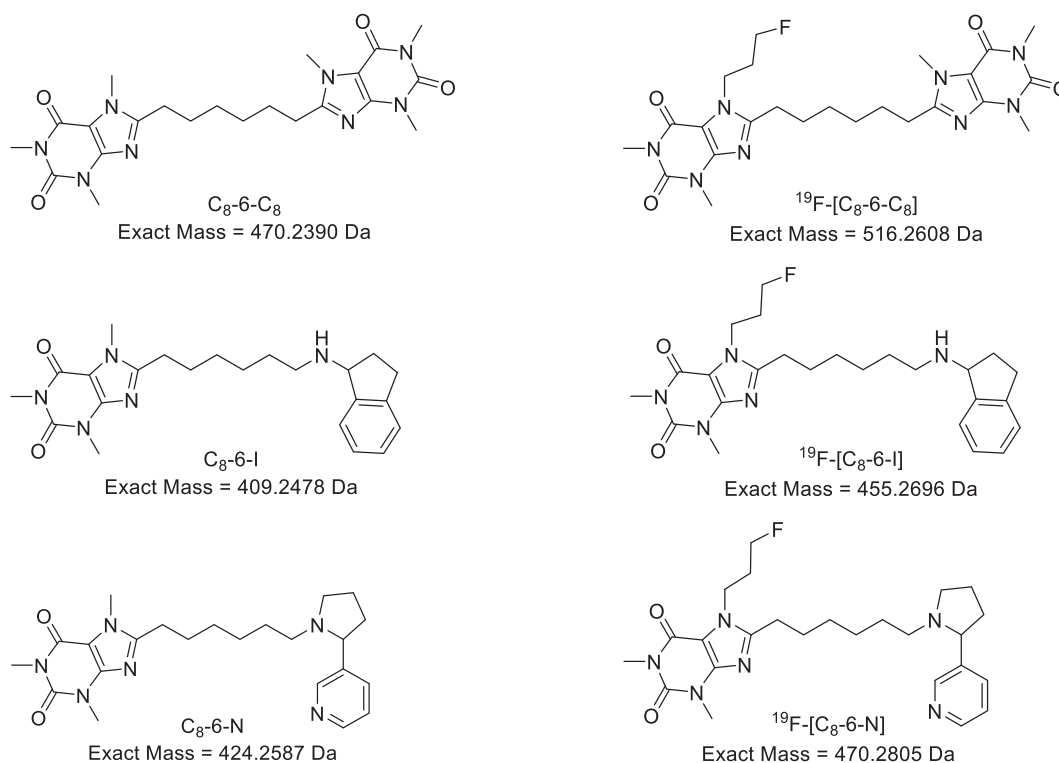


Figure 1. Structure of novel bifunctional compounds and N7-propyl-fluoro analogues.

To develop these bifunctional compounds as therapeutics or diagnostics for Parkinson's disease, it is of great importance to determine their metabolic stability. The metabolism of caffeine (Grant et al. 1987) and nicotine (Murphy 1973; Benowitz et al. 2009) have been previously reported, 1-aminoindan is itself a metabolite of rasagiline, an MAO-B inhibitor (Wang et al. 2016). Caffeine primarily undergoes CYP1A2-mediated *N*-demethylation at three different sites as well as C8 hydroxylation (Grant et al. 1987). The major nicotine metabolite is produced mainly via CYP2A6-mediated metabolism with contribution from CYP2B6 and 2D6 resulting in a 5'-hydroxynicotine that is in equilibrium with an $\Delta^{1(5)}$ iminium ion which is further metabolized by aldehyde oxidase to cotinine (Murphy 1973; Benowitz et al. 2009). How these metabolic pathways will be reflected in the metabolism of C_8 -6-I, C_8 -6-N and C_8 -6- C_8 remains unknown.

Phase 1 metabolic studies utilizing hepatic microsomes *in vitro* are a typical first step in understanding drug metabolism. An advantage of using microsomes as an *in vitro* drug metabolism model is the ability to focus on generating sufficient amounts of presumptive P450-mediated phase I metabolites without contribution from other competing systems such as phase II metabolism and transporter-mediated processes (Temporal et al. 2017). It is our goal to use hepatic microsomes to determine whether our bifunctional compounds undergo Phase 1 metabolism and to identify those metabolic products. Several animal models of Parkinson's disease exist so we have decided to carry out our assessment of *in vitro* metabolism using liver microsomes from several animals (mouse and rat) as well as human liver microsomes. An additional benefit to determining the metabolic stability of our bifunctional compounds is that knowledge of the regiochemistry of metabolic reactions can potentially inform

less metabolically labile positions for incorporation of fluorine in our PET probe bifunctional analogues.

Liquid chromatography coupled with mass spectrometry (LC-MS) is an important analytical platform for the separation, detection, identification, and structural elucidation of metabolites. The identification and structural elucidation of metabolites using LC-MS is achieved through accurate mass measurement and tandem mass spectrometry. Therefore, it is essential to develop an LC method as well as a mass spectrometric method for new chemical entities in preparation for future preclinical studies. Recently, we established a tandem mass spectrometric fingerprint for C_8 -6- C_8 , C_8 -6-I, and C_8 -6-N for future development of qualitative and quantitative methods and these results can be used to inform identification of metabolites (Nwabufo et al. 2019).

The overall goal of this present study is to determine the metabolic profile of C_8 -6- C_8 , C_8 -6-I, C_8 -6-N and their fluorine-labelled analogues in human, mouse, and rat liver microsomes (HLM, MLM, and RLM). This is the first preclinical study to establish the metabolic profile of these compounds in HLM, MLM, and RLM and the information obtained from this study will contribute to the development of these bifunctional compounds as therapeutic or diagnostic agents for Parkinson's disease.

Materials and methods

Chemicals and reagents

C_8 -6-N, C_8 -6-I, and C_8 -6- C_8 were synthesized according to a previously established protocol in our laboratory (Kakish et al. 2016) while 2, 2-di-(3-methoxy methyl phenyl) 1, 3-propanediol (MMPPD) was isolated following a literature method

(Chênevert et al. 1999). Acetonitrile (HPLC grade purity), methanol (HPLC grade purity), chloroform, formic acid (LC/MS grade purity), magnesium chloride ($MgCl_2$) were purchased from Fisher Scientific (Fairlawn, NJ) while water was filtered using a Millipore, MilliQ system with a Quantum EX cartridge (Mississauga, ON). The following chemicals were purchased from Sigma-Aldrich (St. Louis, MO): sodium pyrophosphate decahydrate (SPP), chlorzoxazone, and dipotassium orthophosphate (K_2HPO_4). Potassium dihydrogen orthophosphate (KH_2PO_4) was purchased from BDH Chemicals (Toronto, ON) while reduced nicotinamide adenine dinucleotide (NADPH) was purchased from Roche Diagnostics (Indianapolis, IN). HLM, MLM, and RLM were purchased from Invitrogen (Life Technologies; Burlington, ON).

Non-targeted metabolite identification of C_8-6-C_8 , C_8-6-I and C_8-6-N

The analysis of C_8-6-N , C_8-6-I , and C_8-6-C_8 incubated with microsomes was performed on an Agilent 1100 high-performance liquid chromatography (HPLC) (Agilent technologies; Mississauga, ON) coupled with an AB SCIEX QSTAR XL quadrupole orthogonal time-of-flight hybrid mass spectrometer (QqToF-MS) equipped with an electrospray ionization (ESI) source (AB SCIEX, Redwood City, CA, USA). The Agilent 1100 series HPLC was equipped with a degasser (G1379A), binary pump (G1312A), autosampler (G1329A), and diode array detector (G1315B), and the HPLC column was an Agilent Poroshell 120 EC- C_{18} column (4.6×50 mm, $2.7 \mu m$). The binary solvent system used consisted of 0.1% LC-MS grade formic acid in water (mobile phase A) and 0.1% LC-MS grade formic acid in acetonitrile (mobile phase B), with a flow rate of 0.3 mL/min. A 20-minute gradient elution was set up to ensure separation of the metabolites and parent compounds. The gradient was programmed to start with an initial isocratic hold at 90% mobile phase A for 5 minutes, decreasing gradually to 10% mobile phase A and holding for 10 minutes before returning to the initial conditions at 21 minutes and equilibrating for 5 minutes. The mass spectrometer was operated in the positive ion mode, and nitrogen was used as the ESI nebulizing and drying gas. The instrument was calibrated with a two-point external calibration using caesium iodide (CsI, m/z 132.9049, Sigma-Aldrich, Oakville, ON, Canada) and sex pheromone inhibitor iPD1 (m/z 829.5393, Bachem Bioscience Inc., PA, USA). The ion source voltage was set at 5500 V while the source temperature was optimized and set at 400 °C. The declustering and focussing potential were set at 40 V and 120 V respectively. A scan range of 100-700 m/z was used for metabolite detection.

Identification of metabolites was made by observing unique peaks present in the reaction mixture samples in comparison to the negative control samples. Confirmation of metabolite structure was carried out using accurate mass measurement and tandem mass spectrometry. Tandem mass spectrometric analysis of the observed metabolite ions was performed under the same conditions and set to target the tentative metabolite ions and retention times in order to confirm their fragmentation pattern. The collision energy was

optimized and was set at 25 eV (C_8-6-N), and 17 eV (C_8-6-I) to ensure sufficient fragmentation without depleting the precursor ion. Data analysis was done using Analyst QS 1.1.

Liquid-liquid extraction consisting of a mixture of chloroform-isopropanol (85:15, v/v) was previously used by Grant *et al.*, (Grant et al. 1987) for extraction of caffeine and its metabolites from HLM. Therefore, we evaluated this mixture of solvents for extracting C_8-6-C_8 , C_8-6-N , and C_8-6-I , as well as their corresponding metabolites from HLM, MLM, and RLM but found unacceptably high variation in the results. The variation with acetonitrile was acceptable and was selected as the solvent for protein precipitation.

Single-stage MS and MS/MS analysis of $^{19}F-[C_8-6-C_8]$, $^{19}F-[C_8-6-I]$ and $^{19}F-[C_8-6-N]$

The single-stage MS, MS/MS and multi-stage MS^3 analysis of C_8-6-C_8 , C_8-6-N , and C_8-6-I have previously been reported (Nwabufu et al. 2019). The single-stage MS analysis of $^{19}F-[C_8-6-C_8]$, $^{19}F-[C_8-6-I]$ and $^{19}F-[C_8-6-N]$ were analysed using an AB SCIEX 4000 Q TRAP hybrid triple quadrupole-linear ion trap mass spectrometer (QqLIT-MS) equipped with a turbo spray ESI source (AB Sciex, Redwood City, CA, USA). $^{19}F-[C_8-6-C_8]$, $^{19}F-[C_8-6-I]$ and $^{19}F-[C_8-6-N]$ were infused directly into the mass spectrometer at a flow rate of 10 $\mu L/min$. The turbo ionspray source needle voltage was set to 5500 V with mass spectrometer set to an optimal entrance potential of 10 V and declustering potential of 40 V. Nitrogen was used as the ESI nebulizing (GS1) and drying gas (GS2). The optimal GS1 and GS2 for $^{19}F-[C_8-6-I]$ and $^{19}F-[C_8-6-N]$ was set to 14 psi and 15 psi respectively while the optimal GS1 and GS2 for $^{19}F-[C_8-6-C_8]$ was set to 18 psi and 10 psi respectively.

Tandem mass spectrometric analysis of the three (3) bifunctional compounds was also conducted using AB SCIEX QTRAP 4000 instrument under the same conditions as described for the single-stage MS analysis. Nitrogen was used as the collision gas for CID-MS/MS. The optimized collision energy was 21 eV for the proton adduct of $^{19}F-[C_8-6-I]$, 40 eV for the proton adduct of $^{19}F-[C_8-6-N]$ and 35 eV for the proton adduct of $^{19}F-[C_8-6-C_8]$. The optimized collision exit potential for $^{19}F-[C_8-6-C_8]$, $^{19}F-[C_8-6-I]$ and $^{19}F-[C_8-6-N]$ was set to 10 eV.

Non-targeted metabolite identification of $^{19}F-[C_8-6-C_8]$, $^{19}F-[C_8-6-I]$ and $^{19}F-[C_8-6-N]$

The analysis of incubated $^{19}F-[C_8-6-C_8]$, $^{19}F-[C_8-6-I]$ and $^{19}F-[C_8-6-N]$ was performed on an Agilent 1260 Infinity II HPLC (Agilent technologies; Mississauga, ON) coupled with an AB SCIEX 4000 QTRAP hybrid triple quadrupole-linear ion trap mass spectrometer (QqLIT-MS) equipped with a turbo spray ESI source (AB SCIEX, Redwood City, CA, USA). The Agilent 1260 series HPLC was equipped with a binary pump (G7112B), auto sampler (G7129A) equipped with an integrated sample cooler, column compartment (G7116A), diode array detector WR (G7115A) and same HPLC column as used on the AB SCIEX QSTAR. The binary solvent used is same as that used for non-targeted metabolite identification of C_8-6-

N, C₈-6-I, and C₈-6-C₈. The ion source voltage was set at 5500 V and the source temperature optimized and set at 400 °C. The declustering potential and entrance potential was optimized and set at 40 V and 10 V respectively and scan range of 100 – 850 *m/z* was used for metabolite identification. Identification of metabolites for ¹⁹F-[C₈-6-C₈], ¹⁹F-[C₈-6-I] and ¹⁹F-[C₈-6-N] was carried out as same method used for C₈-6-N, C₈-6-I, and C₈-6-C₈. The collision energy was optimized and set at 22 eV for ¹⁹F-[C₈-6-I], 25 eV for ¹⁹F-[C₈-6-N] and 30 eV for ¹⁹F-[C₈-6-C₈].

Microsomal incubations

A standard method for *in vitro* metabolism of novel bifunctional compounds using liver microsomes was developed and optimized in our laboratory. This method included incubation of chlorzoxazone as a positive control to determine the viability of the liver microsomes. The incubation mixture contained 5 mM MgCl₂, 10 mM SPP, 0.5 mg/mL liver microsomes (rat, mouse or human), and 30 μM test compound. After 5-minute pre-incubation in a shaking water bath at 37 °C, 10 μL NADPH (1 mM final concentration) in pH 7.4 100 mM potassium phosphate buffer was added to initiate the reaction. The incubation mixtures were prepared in duplicate in parallel with two negative controls. The first negative control did not contain NADPH while the second negative control excluded active liver microsomes. The reaction was terminated after 60 minutes by the addition of 200 μL of ice-cold acetonitrile containing 50 μM MMPPD as an internal standard.

The samples were vortexed for about 1 min and then centrifuged at 14000 × *g* for 10 minutes. Subsequently, 200 μL of the supernatant was placed in an LC vial, and 50 μL were injected into the LC-QqToF and 10 μL injected into the LC-QqLIT instrument.

Results and discussion

Metabolites of C₈-6-C₈, C₈-6-I, C₈-6-N

Our first objective was to determine the *in vitro* hepatic metabolites of C₈-6-C₈, C₈-6-I and C₈-6-N in HLM, MLM, and RLM in order to direct our design of ¹⁸F labelled analogues. Since the biotransformation of PET imaging probes can alter the information obtained from biodistribution studies, it was important to perform metabolism studies of these compounds to determine the least metabolically labile position for the attachment of a radioisotope. These first metabolism studies addressed three major questions: are C₈-6-N, C₈-6-I, and C₈-6-C₈ metabolized in HLM, MLM, and RLM; are the metabolic pathways of C₈-6-N, C₈-6-I, and C₈-6-C₈ the same in HLM, MLM and RLM; and what are the least metabolically labile positions for the inclusion of fluorine in C₈-6-N, C₈-6-I, and C₈-6-C₈.

We utilized both accurate mass measurement and tandem mass spectrometric analysis in the identification and structural elucidation of the major P450 metabolites for C₈-6-N, C₈-6-I, and C₈-6-C₈ in HLM, MLM, and RLM. We confirmed the

conversion of chlorzoxazone to 6-hydroxychlorzoxazone as our positive control for microsomal viability. Subsequently, potential metabolites of the bifunctional compounds were selected by comparing the chromatograms of the reaction mixtures against those of the negative control samples (No NADPH and inactive liver microsomes, [Figure S1 Supplementary Information](#)).

We combined the use of QqToF-MS and QqLIT-MS for metabolite identification. Using QqToF-MS, two metabolites (M1, M2) were identified for C₈-6-I ([Figure S1\(A\)](#)), and two metabolites M3 and M4 were identified for C₈-6-N ([Figure S1\(B\)](#)). On the contrary, no metabolite was detected for C₈-6-C₈ ([Figure S1\(C\)](#)) in HLM, MLM, and RLM. We also observed that only C₈-6-N undergoes extensive metabolism in HLM, MLM, and RLM as the parent compound could no longer be detected in the reaction mixture after 60 minutes incubation ([Figure S1\(B\)](#)). These results are summarized in [Table 1](#).

The metabolites were first identified using accurate mass measurement, and the mass error of each of the identified metabolites was less than 7 ppm ([Table S2, Supplementary Information](#)), confirming the molecular structures. These mass accuracies were comparable to the results obtained from previous structural work in which external calibration was used (Nwabufo et al. 2019). Furthermore, MS/MS analysis was performed to confirm the molecular structures of the identified metabolites and to examine how the fragmentation pattern of the identified metabolites relate to the previously established mass spectrometric pattern for C₈-6-N, C₈-6-I, and C₈-6-C₈ (Nwabufo et al. 2019).

When we performed non-targeted metabolite identification with the QqLIT-MS, M3 and M4 of C₈-6-N, identified by accurate mass measurement using QqToF-MS, were also identified using QqLIT-MS. However, for C₈-6-I, in addition to M1 and M2, a third and fourth metabolite M5A and M5B, not detected by QqToF-MS, was detected by QqLIT-MS ([Figure S1\(D\)](#)). This can be due to greater sensitivity of the linear ion trap mass spectrometer in comparison to the time-of-flight mass spectrometer although it is worthwhile to note that M5 has a retention time very close to the parent compound (C₈-6-I).

Metabolites of C₈-6-I

The MS/MS spectrum of metabolite M1 from C₈-6-I ([Figure 2\(A\)](#)) revealed a diagnostic product ion with *m/z* 277.1643 (M1¹) produced by the neutral loss of ammonia (17 Da) from the terminal amino group of the precursor ion at *m/z* 294.1893 ([Figure 2\(A\)](#)). This fragmentation pattern correlates with the previously established fragmentation pathway for C₈-6-I in which fragmentation of C₈-6-I leads to the formation of the product ion with *m/z* 294.4, and subsequent fragmentation leads to the generation of the diagnostic product ion at *m/z* 277.4 with the concomitant loss of ammonia (Nwabufo et al. 2019). Accurate mass measurement revealed that the molecular formula of M1 is C₁₄H₂₄N₅O₂ with a mass error of 0.000 ppm ([Table S2](#)) which correlates with the proposed molecular structure of M1 resulting from N-dealkylation. Together the results obtained from the tandem mass spectrometric analysis and accurate mass measurement

Table 1. Percentage of parent compound remaining after 1 h incubation in HLM, RLM and MLM.

Parent Compounds	% of Parent Compound Remaining after 1 h incubation			Metabolic Reaction
	HLM	RLM	MLM	
C ₈ -6-C ₈	100	100	100	No metabolite detected
¹⁹ F-[C ₈ -6-C ₈]	90.9	61.6	83.3	Propyl fluoride hydroxylation
C ₈ -6-I	36.2	62.4	32.7	Amino-indan hydroxylation, N-dealkylation, N3-demethylation and N1-demethylation
¹⁹ F-[C ₈ -6-I]	77.6	57.4	50.3	Amino-indan hydroxylation, Propyl fluoride hydroxylation N-dealkylation, N3-demethylation and N1-demethylation
C ₈ -6-N	NIL	NIL	NIL	Nicotine hydroxylation, N-dealkylation
¹⁹ F-[C ₈ -6-N]	43.1	52.8	63.2	Nicotine hydroxylation, N-dealkylation

confirmed the molecular structure of M1 (for additional MS details for metabolites of C₈-6-I see Figure S3).

Metabolite M2 of C₈-6-I is 16Da higher than the parent compound consistent with the formation of a hydroxylated metabolite of C₈-6-I. The MS/MS spectrum (Figure 2(B)) of the precursor ion with m/z 426.2539 revealed an abundant diagnostic product ion at m/z 408.2374 (M₂¹) corresponding to the loss of a water molecule (18 Da) from the precursor ion, in agreement with the presence of a hydroxyl group on the precursor ion. The product ion with m/z 294.1917 (M₂²) is also diagnostic for the parent compound (C₈-6-I), indicating that the precursor ion [M₂ + H]⁺ originated from C₈-6-I. M₂² is formed from the loss of hydroxyindene from the precursor ion [M₂ + H]⁺ suggesting that the hydroxyl group is located on the indan moiety of M2. The neutral loss of C₁₄H₂₃N₅O₂ (293 Da) from [M₂ + H]⁺ is associated with the formation of the product ion at m/z 133.0583 (M₂³). A neutral loss of C₁₄H₂₃N₅O₂ (293 Da) from C₈-6-I is associated with the formation of a protonated indene and the protonated indene formed from this loss is 16Da higher than M₂³, a strong indication that the hydroxyl group is located on the indan moiety of M2.

Although the fragmentation pattern suggests that the hydroxyl group is located on the indan moiety of M2, it does not indicate the position in which it is located on the indan moiety. However, previous studies suggest that rasagiline (a monoamine oxidase-B inhibitor used in the treatment of Parkinson's disease) undergoes P450 mediated biotransformation to 1-aminoindan, and subsequent P450 mediated metabolism of 1-aminoindan results in hydroxylation at the benzyl position leading to the formation of 3-hydroxy-1-aminoindan (Deftereos et al. 2012; Agundez et al. 2013; de Biase et al. 2014); hydroxylation at the benzyl position adjacent to the amine leads to N-dealkylation as observed for M1. This suggests that carbon 3 of the indan is likely the position of hydroxylation on M2 however, further structural characterization studies will be necessary to confirm this. Furthermore, accurate mass measurement revealed the molecular formula of M2 as C₂₃H₃₂N₅O₃ with a mass error of 6.8035 ppm (Table S2), confirming the projected molecular structure.

The minor metabolites M5A and M5B, both with m/z 396.24, are consistent with the loss of a methyl group (14 Da). Previous *in vitro* metabolism studies indicate that caffeine undergoes phase 1 metabolism to generate four primary metabolites: paraxanthine (major), theobromine, theophylline, and 1, 3, 7-trimethyluric acid which correspond to N3, N1, N7- demethylation, and C8-oxidation respectively

(Ferrero and Neims 1983; Campbell et al. 1987; Grant et al. 1987; Berthou et al. 1989). The product ion of metabolites M5A and M5B undergoes fragmentation (Figure 2(C,D), Figure S3) that leads us to conclude that formation of M5A and M5B is most likely N1 and N3 demethylation, respectively, similar to the formation of theobromine and paraxanthine as major metabolites for caffeine.

The MS/MS spectrum (Figure 2(C)) of the precursor ion with m/z 396.24 revealed an abundant diagnostic product ion with m/z 280.21 (M₅¹) corresponding to the loss of indene (117 Da) from the precursor ion. We previously established that loss of indene from C₈-6-I resulted in the product ion m/z 294.19 (Nwabufu et al. 2019), and since M₅¹ (m/z 280.21) is 14 Da less, this indicates demethylation occurs on the caffeine moiety of C₈-6-I. Another major diagnostic product ion at m/z 263.27 (M₅²) corresponds to the neutral loss of ammonia from the terminal group of M₅¹, which also correlates with the established fragmentation pattern of C₈-6-I. Product ion M₅³ at m/z 249.27 corresponds to loss of methyl amine from M₅² (m/z 263.27) and M₅⁴ (m/z 237.31) is the result of loss of isocyanic acid (O=C=NH, 43 Da) from precursor ion M₅¹. Typically for fragmentation of C₈-6-I, the loss of methyl isocyanate (O=C=NCH₃, 57 Da) is observed, however we observe both the loss of isocyanic acid (M₅⁴) and methyl isocyanate (M₅⁷) (Figure S3) from the caffeine moiety confirming that the precursor ion of M5 at m/z 396.24 is a metabolite from C₈-6-I. Product ion M₅⁵ with m/z 193.20 corresponds to loss of 1-pentene (C₅H₁₀, 70 Da) from (M₅²), while M₅⁶ with m/z 117.05 is 2, 3-dihydro-1H-inden-1-ylum (C₉H₉⁺) formed by neutral loss of C₁₃H₂₁N₅O₂ (279 Da) from [M₅ + H]⁺. The fragmentation pattern of [M₅ + H]⁺, most notably the loss of isocyanic acid and methyl isocyanate, suggests that the demethylation of C₈-6-I is analogous to N1 and N3 demethylation of caffeine to theobromine and paraxanthine respectively. The neutral loss of isocyanic acid with 43 Da is a neutral loss associated with the fragmentation of theobromine and the neutral loss of methyl isocyanate with 57 Da is associated with fragmentation of paraxanthine (Mendes et al. 2019).

1-Aminoindan is a P450 metabolite of the Parkinson's disease therapeutic rasagiline and, 1-aminoindan can be further metabolized to 3-hydroxy-1-aminoindan (Deftereos et al. 2012; Agundez et al. 2013; de Biase et al. 2014). We identified a hydroxylated metabolite of C₈-6-I and tandem mass spectrometric analysis suggests that the hydroxyl group is located on the 1-aminoindan moiety, what is less clear is the position of hydroxylation on the 1-aminoindan

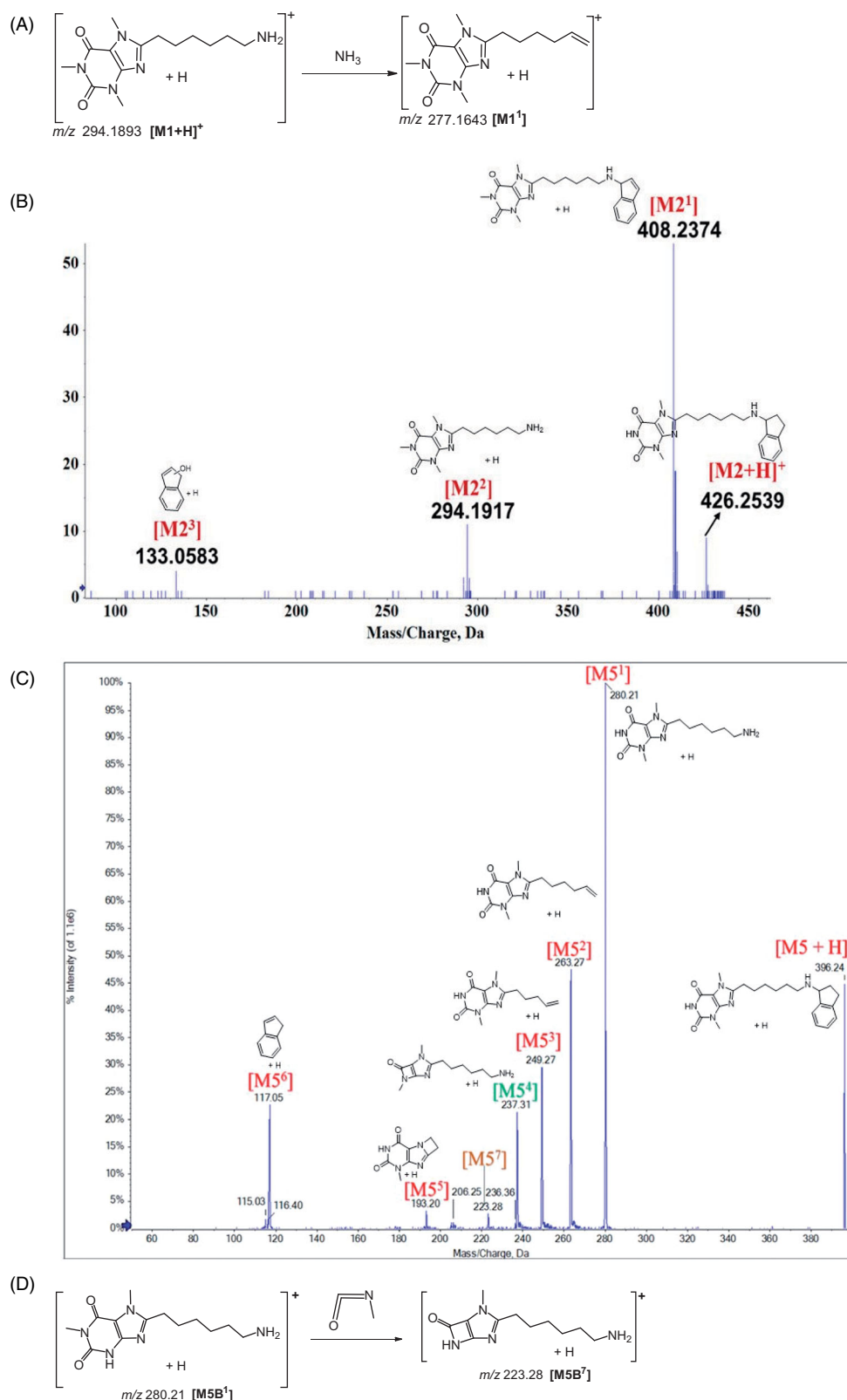


Figure 2. (A) Proposed fragmentation pathway for C₈-6-I metabolite M1. (B) The ESI-QToF-MS/MS spectrum and the proposed fragments for C₈-6-I metabolite M2. (C) The ESI-QqLIT-MS spectrum and the proposed fragments for C₈-6-I metabolites M5. (D) Proposed fragmentation pathway for C₈-6-I metabolite M5B. ESI was performed in positive mode.

moiety. We have proposed reactions for the dealkylation and hydroxylation of C₈-6-I (Figure 4(A)). Dealkylation requires initial hydroxylation to occur at the 1-position followed by breakdown of the carbinolamine to form M1 with the

concomitant loss of 1-oxoindan (Figure 4(A)). Hydroxylation of C₈-6-I is more likely to occur at the benzylic 3-position to give M2. It has been suggested that 3-hydroxy-1-aminoindan may have neuroprotective effects (Sterling et al. 1998),

therefore M2 may also be neuroprotective. Additionally, given that M1 still contains the caffeine moiety, it may also possess neuroprotective properties.

Metabolism of C₈-6-N

The M3 metabolite of C₈-6-N has a similar fragmentation pathway as the M1 metabolite of C₈-6-I (Figure 2(A)). The molecular formula and mass error of M1 and M3 are the same indicating that they both have the same molecular structure, pointing to an N-dealkylation of the nicotine moiety. Another metabolite of C₈-6-N (M4) is 16 Da higher than the parent compound consistent with hydroxylation. The MS/MS spectrum of M4 (Figure 3(A)) shows an abundant diagnostic product ion at *m/z* 423.2557 (M4¹) originating from the neutral loss of a water molecule from the precursor ion at *m/z* 441.2713 [M4 + H]⁺ consistent with the presence of a hydroxyl group on the precursor ion [M4 + H]⁺. Subsequent fragmentation of [M4 + H]⁺ is linked to the neutral loss of C₉H₁₂N₂O (164 Da) with the concomitant formation of the diagnostic product ion at *m/z* 277.1667 (M4²). This diagnostic neutral loss of C₉H₁₂N₂O (164 Da) leading to M4² suggests that the hydroxyl group is located on the nicotine moiety of the M4. Additionally, M4² is one of the product ions of C₈-6-N, and its presence in the MS/MS spectrum of M4 suggests that M4 originated from C₈-6-N. Finally, the diagnostic product ion at *m/z* 148.0783 (M4³) is formed from the loss of C₁₄H₂₃N₅O₂ (293 Da) from the precursor ion at *m/z* 441.2713. The presence of a hydroxyl group in M4³ strongly suggests that the hydroxyl group is located on the nicotine moiety of M4.

Both 2' and 5' phase I hydroxylated metabolites of nicotine have been reported (Murphy 1973; Brandange and Lindblom 1979; Peterson et al. 1987; Hecht et al. 2000) suggesting that M4 was hydroxylated at either the 2' or 5' position of nicotine. Indeed, the formation of M3 (N-dealkylation product) would require hydroxylation to have occurred at both the 2' and 5' positions of nicotine increasing the likelihood that M4 is the result of hydroxylation at one of these

positions; further structural characterization studies will be necessary to determine the exact position in which the hydroxyl group is located on M4. Furthermore, accurate mass measurement revealed the molecular formula of M4 as C₂₃H₃₃N₆O₃ with a mass error of 6.1188 ppm (Table S2), confirming the projected molecular structure. It should also be noted that if 2' or 5' hydroxylation has occurred the hydroxylated structure may be in equilibrium with the ring-opened ketone or aldehyde respectively (Figure 4(B)).

Nicotine undergoes *in vitro* P450-mediated metabolism resulting in the formation of: nicotine-Δ^{1'}(5')-iminium ion, 5'-hydroxynicotine, nornicotine, 2'-hydroxynicotine, 4-(methylamino)-1-(3-pyridyl)-1-butanone, 4-oxo-4-(3-pyridyl) butanoic acid and 4-hydroxy-4-(3-pyridyl) butanoic acid (Benowitz et al. 2009). Given that 70-80% of nicotine is biotransformed to cotinine and the 5'-hydroxylation pathway leads to the formation of cotinine by a cytoplasmic aldehyde oxidase-mediated reaction (Benowitz et al. 2009), we propose that the hydroxyl group on M4 is most likely located on the 5'-position of the nicotine moiety (Figure 4(B)). Since microsomes do not contain cytoplasmic enzymes such as aldehyde oxidase, a 5'-hydroxylated metabolite of C₈-6-N cannot be converted to cotinine. We propose that the mechanism of formation of M3 is based on ring opening dealkylation which occurs at the 5'-hydroxy position followed by dealkylation at the 2'-hydroxy position resulting in loss of 4-oxo-4-pyridyl butanal.

Furthermore, previous studies suggest that nicotine and some of its metabolites (such as cotinine) have neurotherapeutic effects for Parkinson's disease (Barreto et al. 2014). This suggests that M4 may have similar neuroprotective effect as the parent compound (C₈-6-N). More so, 2'-hydroxylation of nicotine is an important step in the formation of 4-(methylamino)-1-(3-pyridyl)-1-butanone, 4-oxo-4-(3-pyridyl) butanoic acid and 4-hydroxy-4-(3-pyridyl) butanoic acid (Hecht et al. 2000); however, this is a minor pathway in nicotine metabolism. In fact, this pathway is toxicologically significant since 4-(methylamino)-1-(3-pyridyl)-1-butanone can

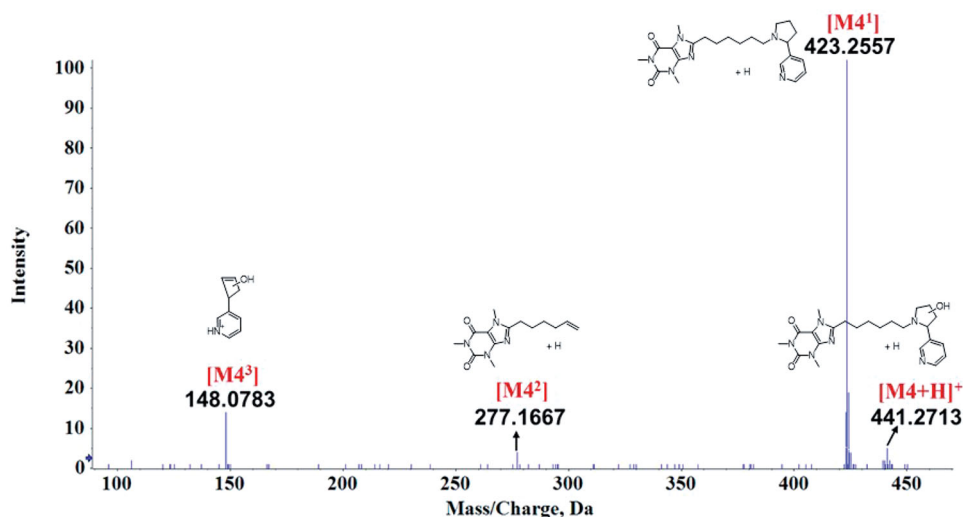


Figure 3. The ESI-QToF-MS/MS spectrum for C₈-6-N metabolite M4(A), and the proposed fragments for M4(B). ESI was performed in positive mode.

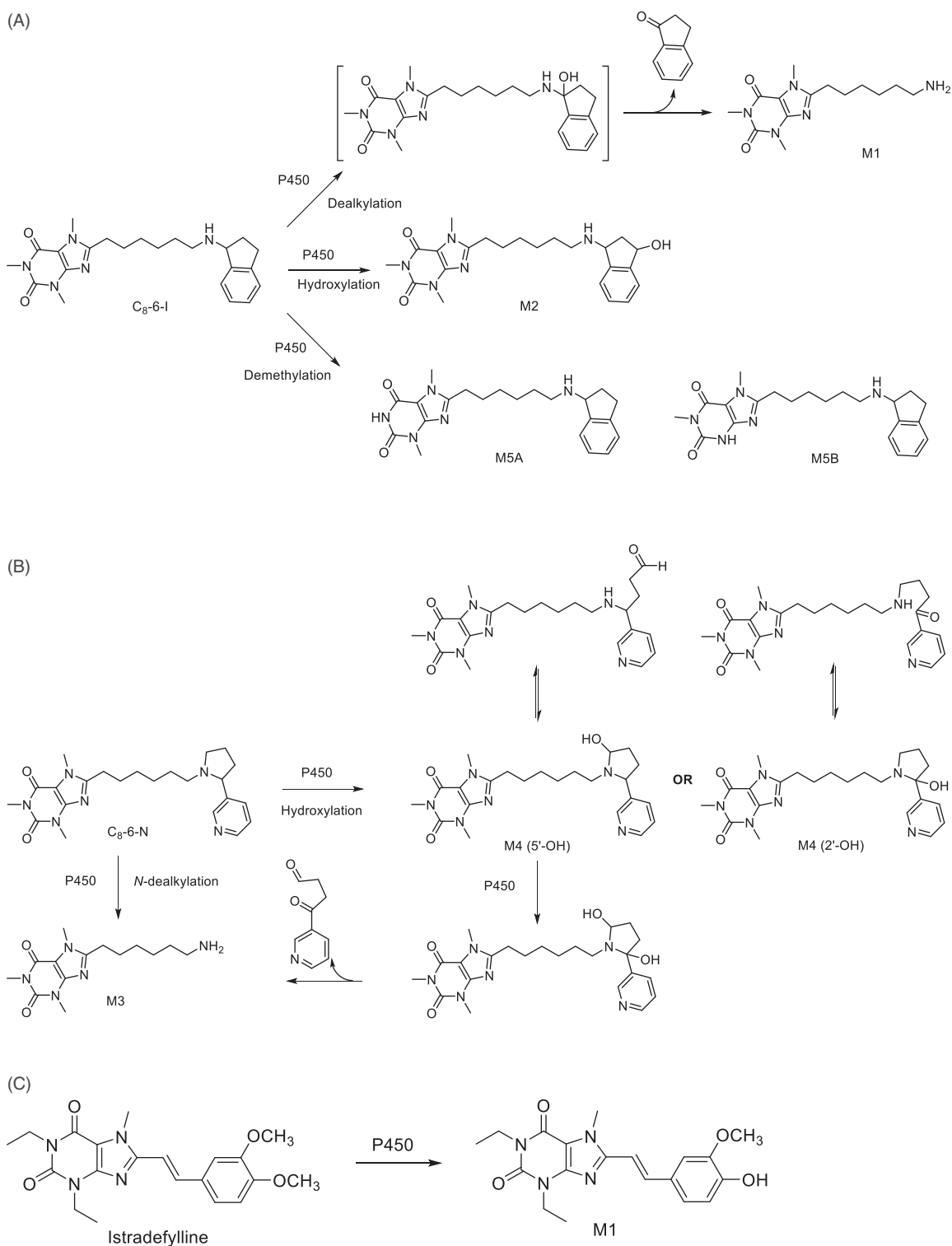


Figure 4. The proposed metabolic pathway for (A) C_8-6-I and (B) C_8-6-N in human, mouse, and rat liver microsomes. (C) Primary phase I metabolic pathway of Istradefylline.

be biotransformed to carcinogenic 4-(methylnitrosamino)-1-(3-pyridyl)-1-butanone (NNK) (Benowitz et al. 2009). Fortunately, this pathway was not observed in the biotransformation of C_8-6-N in HLM, RLM, and MLM.

Metabolism of C_8-6-C_8

We were unable to detect the formation of metabolites for C_8-6-C_8 in HLM, MLM, or RLM (Figure 4(C)). Since C_8-6-N , C_8-6-I , and C_8-6-C_8 all have a caffeine moiety in common, we

expected that caffeine metabolism could be the common metabolic pathway for these bifunctional compounds however, this was not the case. Indeed, we observed that the caffeine moiety of C₈-6-N and C₈-6-C₈ was unchanged and only underwent minimal biotransformation in C₈-6-I. We had previously noted a greater energetic stability for C₈-6-C₈ from our tandem mass spectrometric analysis as more collision energy was required for complete dissociation of C₈-6-C₈ compared to C₈-6-N and C₈-6-I (Nwabufu et al. 2019). This observation leads us to speculate that dimerization of the caffeine monomer might have conferred energetic stability to C₈-6-C₈ which also rendered it more resistant to P450 metabolism. The low *in vitro* turnover rate of the enzymes involved in the metabolism of caffeine (Grant et al. 1987; Berthou et al. 1988) may also be responsible for the metabolic stability of C₈-6-C₈, as well as the caffeine moiety of C₈-6-N. Previously we observed that C₈-6-C₈ did not protect yeast cells and may have been toxic, even though caffeine was found to prevent α -synuclein mediated toxicity in a yeast model of Parkinson's disease (Kakish et al. 2016). Whether toxicity is the result of the lack of P450 metabolism leading to diminished clearance of C₈-6-C₈ is unknown. In line with our observations, istradefylline, a caffeine analogue that is currently used in combination with levodopa/carbidopa for the treatment of Parkinson's disease, was reported to be primarily eliminated by oxidative metabolism on the non-caffeine moiety with the main metabolite being M1 (4'-O-monodesmethylated) (Mukai et al. 2018) (Figure 4(C)) further supporting the idea that C8 functionalization of caffeine may confer metabolic stability.

It is important to acknowledge that our *in vitro* metabolism study serves as an initial screening mechanism to rule out any insignificant metabolic pathways and to further direct *in vivo* testing (Jia and Liu 2007). Certain factors for *in vivo* testing that are not accounted for in this study include the absence of cytosolic enzymes and cofactors to support the generation of phase II metabolites, as well as xenobiotic transporters.

In order for these novel bifunctional compounds to be developed as imaging probes with clinical translation for treatment or diagnosis of Parkinson's disease, they will be required to display high binding affinity, specificity, sensitivity, contrast ratio to α -synuclein, as well as low immunogenicity and toxicity (Chen and Chen 2010). The metabolic stability of these compounds can alter their binding affinity, sensitivity, selectivity and toxicity however, our *in vitro* metabolism studies suggest that the caffeine moiety of these bifunctional agents is metabolically stable and is the most appropriate location for incorporation of an ¹⁸F radioisotope. Based on these results we have prepared a series of N-7 linked fluorine labelled analogues.

¹⁹F-[C₈-6-C₈], ¹⁹F-[C₈-6-I] and ¹⁹F-[C₈-6-N]

Synthesis of ¹⁹F-[C₈-6-C₈], ¹⁹F-[C₈-6-I] and ¹⁹F-[C₈-6-N]

We designed ¹⁹F-labelled analogues of our bifunctional compounds based on the *in vitro* metabolism studies of C₈-6-C₈, C₈-6-I and C₈-6-N that indicated the relative stability of the

caffeine moiety to Phase I metabolism. The scaffold for synthesis of ¹⁹F-[C₈-6-C₈], ¹⁹F-[C₈-6-I] and ¹⁹F-[C₈-6-N] was prepared following our previous method (Kakish et al. 2016). We added a propyl-fluoro linker at N7 of theophylline (caffeine precursor) of our scaffold either via introduction of an iodinated propyl group (prepared as shown in Figure 5(A)) for ¹⁹F-[C₈-6-C₈] and ¹⁹F-[C₈-6-I] followed by fluorination with tertiary butyl ammonium fluoride (TBAF) (Figure 5(B,C)) or introduction of the propyl linker with the terminal fluorine already present (¹⁹F-[C₈-6-N]) as outlined in Figure 6 (for synthetic details see Figure S14). We chose to use a propyl linker rather than an ethyl linker as preliminary experiments indicated that elimination yielding an alkene was the major product instead of fluorination when using the ethyl linker.

MS/MS analysis of ¹⁹F-[C₈-6-C₈], ¹⁹F-[C₈-6-I] and ¹⁹F-[C₈-6-N]

Previously, we demonstrated that the MS/MS analysis of C₈-6-C₈, C₈-6-I and C₈-6-N showed distinct fragmentation patterns (Nwabufu et al. 2019), these results have been used in the preceding sections to guide identification of their *in vitro* metabolites. In our previous study we noted that C₈-6-C₈ required a higher collision energy than C₈-6-N and C₈-6-I, suggesting that the caffeine moiety may be more stable during collision-induced dissociation (CID-MS/MS) analysis. Now we have performed CID-MS/MS of ¹⁹F-[C₈-6-C₈], ¹⁹F-[C₈-6-I] and ¹⁹F-[C₈-6-N] for comparison of their fragmentation pattern to C₈-6-C₈, C₈-6-I and C₈-6-N and to guide our identification of the metabolites of the ¹⁹F-labelled analogues.

We hypothesize that the fragmentation pattern of the fluorinated analogues compounds will resemble that of the non-fluorinated bifunctional compounds. Interestingly, the fluorinated bifunctional compounds required less collision energy to induce fragmentation than their non-fluorinated counterparts indicating that the addition of propyl fluoride to the N-7 position of the caffeine moiety influences fragmentation.

MS/MS analysis of ¹⁹F-[C₈-6-C₈]

The MS/MS spectrum, as well as the proposed fragmentation pathway for the singly charged [M + H]⁺ ion of ¹⁹F-[C₈-6-C₈] with *m/z* 517.43 are shown in Figure S4(A,B). The proposed fragmentation pathway is based on our previously reported fragmentation pathway for C₈-6-C₈ (Nwabufu et al. 2019). The predominant product ion at *m/z* 497.33 is associated with a neutral loss of hydrogen fluoride (-HF, 20 Da) to form a terminal stable alkene. The intensity of this product ion makes it very useful in qualitative analysis of *in vitro* metabolism of ¹⁹F-[C₈-6-C₈]. The predominant product ion at *m/z* 497.33 Da dissociates into the following ions: *m/z* 301.25 associated with the loss of caffeine (C₈H₁₀N₄O₂, 194 Da) and H₂ (2 Da), *m/z* 440.31 associated with a loss of methyl isocyanate (O=C=NCH₃, 57 Da) by reverse Diels-Alder rearrangement, and *m/z* 383.26 and associated loss of 2 molecules of methyl isocyanate [2(O=C=NCH₃), 114 Da] (Figure S4(B)).

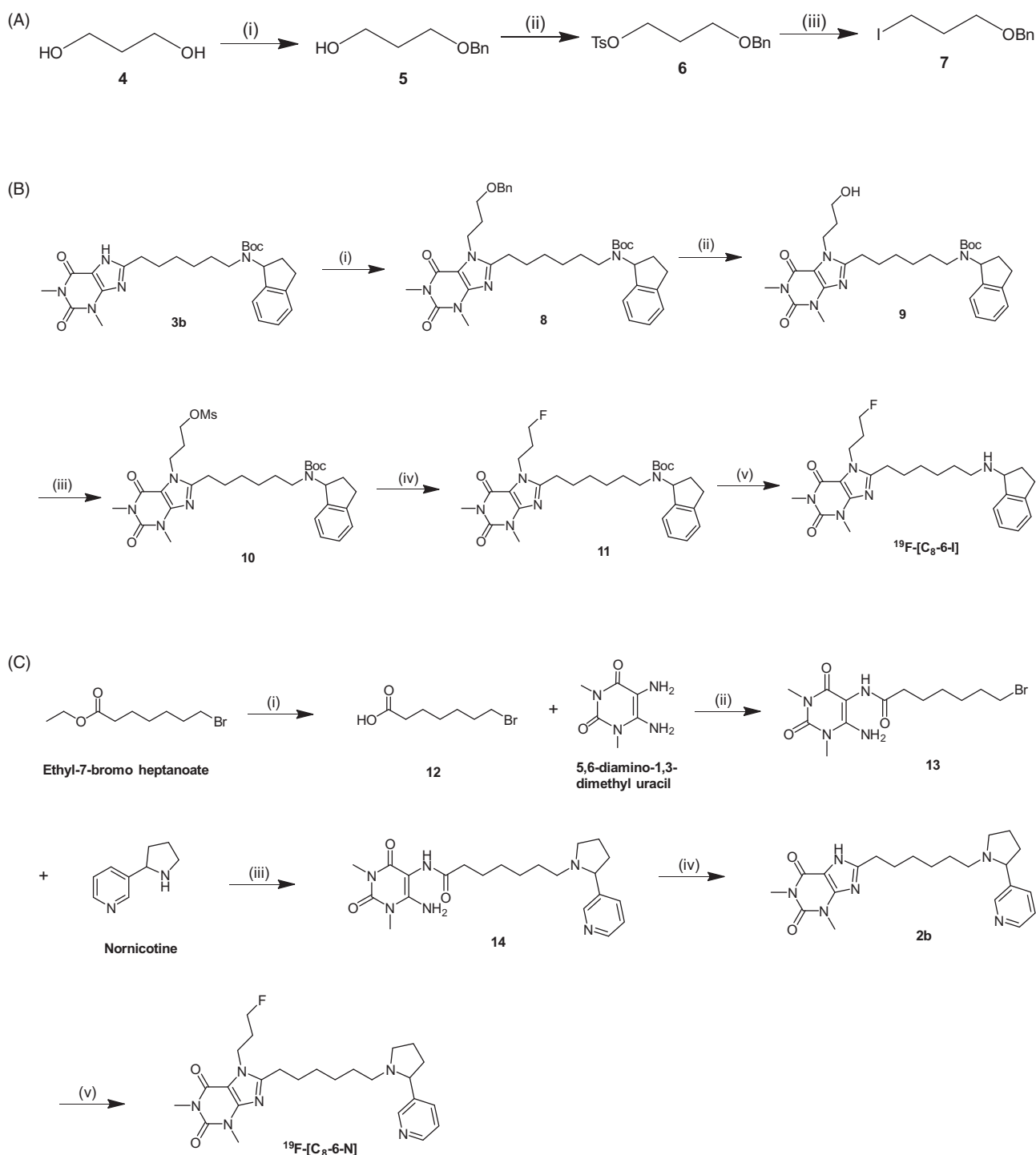


Figure 5. (A) Synthesis of 3-benzyloxy iodopropane. Reagents and conditions: (i) NaH, BnBr, 18 h, 0 °C – 100 °C, 100%; (ii) TsCl, Et₃N, CH₂Cl₂, 12 h, room temp., 72%; (iii) NaI, Acetone, 9 h, room temp – reflux, 72%. (B) Synthesis of ¹⁹F-[C₈-6-I]. Reagents and conditions: (i) 7, K₂CO₃, THF, 72 h, reflux, 69%; (ii) 10% Pd/C, THF, 9 h, room temp., 52%; (iii) MsCl, Et₃N, CH₂Cl₂, 2 h, 0 °C, 79%; (iv) TBAF, CH₃CN, 0.5 h, 80 °C, 73%; (v) 4 N HCl, CH₂Cl₂, 1.5 h, room temp, 65%. (C) Synthesis of ¹⁹F-[C₈-6-N]. Reagents and conditions: (i) 2 N LiOH, CH₃OH, 1 h, room temp., 89%; (ii) EDCI.HCl, CH₃OH, 24 h, room temp, 45%; (iii) DIPEA, CH₃CN, 21 h, 65 °C, 93%; (iv) 10% NaOH, CH₃OH, 18 h, 85 °C, 85%; (v) 1-iodo-3-fluoro propane, Cs₂CO₃, THF, 22 h, reflux, 79%.

The product ion at m/z 473.41 is derived from the neutral loss of carbon dioxide (CO₂, 44 Da) and the product ion at m/z 460.19 is derived from the neutral loss of methyl isocyanate (O=C=NCH₃, 57 Da) as a result of a reverse Diels-Alder rearrangement from the singly charged [M + H]⁺ ion consistent with previously reported fragmentation mechanisms of caffeine (Bianco et al. 2009; Bier et al. 2013) and C₈-6-C₈ (Nwabufu et al. 2019).

Product ions of m/z 233.1 and 194.10 result from the loss of hydrogen fluoride (-HF, 20) in addition to fragmentation of the caffeine backbone structures C₁₃H₁₆N₄O₂ (260 Da) and C₁₅H₂₁N₅O₂ (303 Da) respectively, from m/z 517.43 [M + H]⁺. The product ion at m/z 194.10 further undergoes reverse Diels-Alder rearrangement characterized by loss of methyl isocyanate (O=C=NCH₃, 57 Da) to give the ion at m/z 137.16 (Figure S4(B)). Three other fragmentation pathways

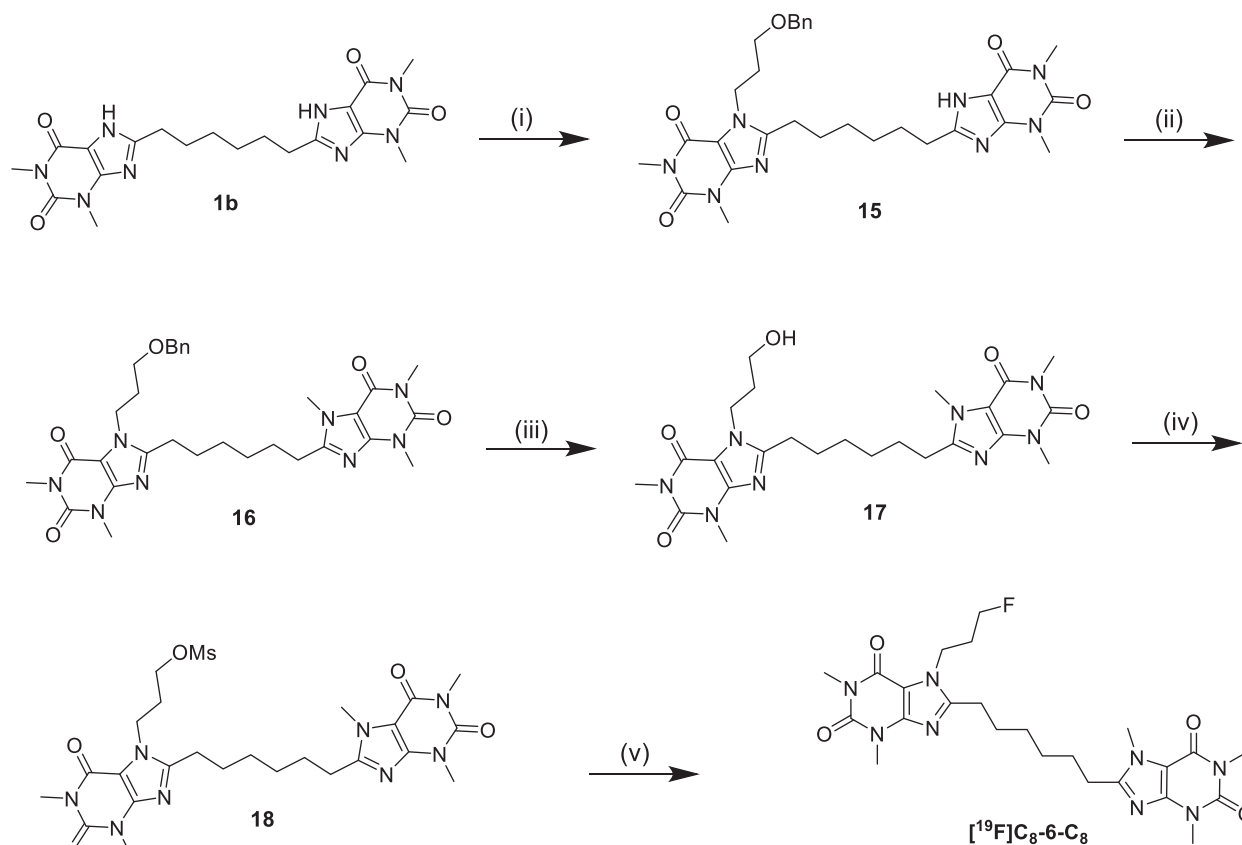


Figure 6. Synthesis of ^{19}F -[C₈-6-C₈]. Reagents and conditions: (i) 7, K₂CO₃, DMSO, 18 h, 50 °C, 45%; (ii) CH₃I, K₂CO₃, THF/DMSO, 18 h, 50 °C, 72%; (iii) 10% Pd/C, H₂, THF/DMF, 18 h, room temp, 57%; (iv) MsCl, Et₃N, CH₂Cl₂, 0.5 h, 0 °C, 63%; (v) TBAF, CH₃CN, 0.5 h, 80 °C, 63%.

from the singly charged m/z 517.43 $[\text{M} + \text{H}]^+$ ion involve the loss of hydrogen fluoride (-HF, 20 Da) and C₁₁H₁₂N₄O₂ (232 Da). In the first instance a product ion with m/z 263.21 is formed however, additional loss of H₂ (2 Da) gives product ion m/z 261.08, whereas loss of methyl isocyanate (O=C=NCH₃, 57 Da) results in the product ion at m/z 208.23.

MS/MS analysis of ^{19}F -[C₈-6-I]

The MS/MS spectrum, as well as the proposed fragmentation pathway for the singly charged $[\text{M} + \text{H}]^+$ ion of ^{19}F -[C₈-6-I] with m/z 456.32 are shown in Figure S5(A,B). The fragmentation gives rise to the major product ion at m/z 340.28 characterized by the neutral loss of indene (C₉H₈, 116 Da) as shown in Figure S5(B), which is very similar to the major product ion seen in the fragmentation of C₈-6-I (M5A¹, Figure 2(C)). We noted that the 1-aminoindan bond appears to be the weakest bond for collision-induced dissociation of ^{19}F -[C₈-6-I]. This is in contrast to our observations for ^{19}F -[C₈-6-C₈] and ^{19}F -[C₈-6-N] where fragmentation is largely dominated by the loss of hydrogen fluoride (-HF, 20 Da) from the carbon-fluorine bond. The product ion at m/z 340.28 further dissociates by neutral loss of hydrogen fluoride (-HF, 20 Da) to give a product ion at m/z 320.26. A small intensity product ion at m/z 436.32 is associated with the neutral loss of hydrogen fluoride (-HF, 20 Da) from the singly charged $[\text{M} + \text{H}]^+$ ion of ^{19}F -[C₈-6-I] (Figure S5(B)). The product ion at m/z 117.13 (2,3-dihydro-1H-inden-1-ylum (C₉H₉⁺)) is

associated with neutral loss of C₁₆H₂₆FN₅O₂ (339 Da) from the singly charged $[\text{M} + \text{H}]^+$ ion of ^{19}F -[C₈-6-I].

MS/MS analysis of ^{19}F -[C₈-6-N]

The MS/MS spectrum, as well as the proposed fragmentation pathway for the singly charged $[\text{M} + \text{H}]^+$ ion of ^{19}F -[C₈-6-N] with m/z 471.29 are shown in Figure S6(A,B). The proposed fragmentation pathway is based on our previously reported fragmentation pathway for C₈-6-N (Nwabufo et al. 2019). Similar to ^{19}F -[C₈-6-C₈], the predominant product ion at m/z 451.32 is derived from the neutral loss of hydrogen fluoride (-HF, 20 Da) (Figure S6(A)) indicating that the alkyl fluoride moiety is the weakest bond and this fragmentation path may be useful in metabolite identification with MS/MS analysis. Only three product ions (m/z 263.14, 194.11 and 137.19) were observed in which the caffeine portion underwent dissociation, similar to what we previously reported for C₈-6-N, thus fragmentation of ^{19}F -[C₈-6-N] is largely dominated by dissociation of the nicotine moiety.

The product ion at m/z 392.25 is associated with the loss of pyridine (C₅H₅N, 79 Da) in agreement with previously reported MS/MS analysis of nicotine (Medana et al. 2016) while the product ion at m/z 372.25 is associated with the loss of hydrogen fluoride (-HF, 20 Da) and pyridine (C₅H₅N, 79 Da). The product ion at m/z 372.25 further dissociates into three product ions: m/z 303.23 and m/z 301.17 associated with the loss of dihydropyrrrole (C₄H₇N, 69 Da) and further loss of H₂ (2 Da) respectively; and the neutral loss of 7-(2, 3-

dihydro-1*H*-pyrrol-1-yl) heptanenitrile (C₁₁H₁₈N₂, 178 Da) gives rise to the ion at *m/z* 194.11 (Figure S6(B)). The product ion at *m/z* 332.22 is associated with the loss of hydrogen fluoride (-HF, 20 Da) and 3-(1-prop-1-en-1-yl) pyridine (C₈H₉N, 119 Da), while the product ion at *m/z* 263.14 appears to result from the loss of hydrogen fluoride (-HF, 20 Da), methyl isocyanate (O=C=NCH₃, 57 Da) and 3-(cyclobut-2-en-1-yl) pyridine (C₉H₉N, 131 Da) and this product ion undergoes further loss of 7-aminoheptanenitrile (C₇H₁₄N₂, 126) to give the ion at *m/z* 137.19. The product ion at *m/z* 323.22 is consistent with loss of nornicotine (C₉H₁₂N₂, 148 Da).

The remaining product ions derived directly from the singly charged [M + H]⁺ ion of ¹⁹F-[C₈-6-N] are consistent with fragmentation of the nicotine moiety (Figure S6(B)). Product ions at *m/z* 132.08, 130.11, 120.16 and 106.11 all result from neutral losses of the caffeine backbone structure of ¹⁹F-[C₈-6-N] in agreement with previously reported fragmentation of nicotine (Medana et al. 2016) and C₈-6-N (Nwabufu et al. 2019).

Metabolite profiling of ¹⁹F-[C₈-6-I], ¹⁹F-[C₈-6-C₈] and ¹⁹F-[C₈-6-N]

Once we successfully prepared the ¹⁹F-labelled analogues, the major goal of the second part of this study was to determine the metabolic fate of ¹⁹F-[C₈-6-I], ¹⁹F-[C₈-6-C₈] and ¹⁹F-[C₈-6-N] in HLM, MLM and RLM. To accomplish this the ¹⁹F analogues were incubated under the same conditions as the unlabelled bifunctional agents. We then used tandem mass spectrometric analysis together with the mass spectrometric fingerprints of the non-fluorinated and fluorinated bifunctional compounds to identify the major presumptive P450 metabolites for ¹⁹F-[C₈-6-I], ¹⁹F-[C₈-6-C₈] and ¹⁹F-[C₈-6-N]. Five metabolites (M6, M7A, M7B and M8A, M8B) were identified for ¹⁹F-[C₈-6-I] (Figure S7(A)), one metabolite was identified for ¹⁹F-[C₈-6-C₈] (Figure S7(B)) and two metabolites were identified for ¹⁹F-[C₈-6-N] in HLM, MLM and RLM (Figure S7). The results are summarized in Table 1.

Metabolism of ¹⁹F-[C₈-6-I]

The MS/MS spectrum of metabolite M6 derived from ¹⁹F-[C₈-6-I] (*m/z* 340.19 [M6 + H]⁺), reveals several diagnostic product ions (Figure S10(A)). The first diagnostic product ion of [M6 + H]⁺ is M6² at *m/z* 320.28 produced from neutral loss of hydrogen fluoride (-HF) from the precursor ion (Figure S10(B)). This correlates with the fragmentation pattern of ¹⁹F-[C₈-6-I] (see Figure S5(A,B)) where fragmentation of the parent compound leads to the formation of a product ion at *m/z* 340.28, and subsequent fragmentation via loss of hydrogen fluoride to generate a diagnostic product ion at *m/z* 320.26. Another diagnostic product ion (M6¹) at *m/z* 323.27, corresponds to the loss of a terminal ammonia from the precursor ion at *m/z* 340.19. These two diagnostic product ions M6² and M6¹ derived from precursor ion *m/z* 340.19 are consistent with [M6 + H]⁺ resulting from metabolic N-dealkylation of ¹⁹F-[C₈-6-I], which is in agreement with N-dealkylation observed for C₈-6-I metabolism. Another product ion (M6³)

at *m/z* 303.33 indicates both the loss of hydrogen fluoride and ammonia from precursor ion *m/z* 340.19. M6³ subsequently fragments to give M6⁸ at *m/z* 194.28 and M6⁵ at *m/z* 246.34 which correspond to the loss of 6-heptanenitrile and methyl isocyanate respectively. The formation of M6⁵ at *m/z* 246.34 is followed by a subsequent loss of 6-heptanenitrile to give a product ion (M6⁹) at *m/z* 137.27. M6⁴ at *m/z* 263.34 is a product ion resulting from loss of methyl isocyanate from M6² (*m/z* 320.28) followed by the subsequent loss of methyl amine and ethyl amine to give M6⁶ (*m/z* 232.37) and M6⁷ (*m/z* 218.35) respectively. The complete fragmentation pattern of [M6 + H]⁺ suggests to us that M6 is an N-dealkylated metabolite of ¹⁹F-[C₈-6-I] in which the indan moiety has been lost.

M7A and M7B are two metabolites with the same retention time and same *m/z* of 472.32 which is 16 Da more than the parent compound (¹⁹F-[C₈-6-I], *m/z* 456.32) which corresponds to hydroxylation of the parent compound. However, the fragmentation spectrum of [M7 + H]⁺ (Figure S5(C)) to produce diagnostic product ions revealed that there are two distinct fragmentation pathways suggesting the presence of two different mono-hydroxylated metabolites. The fragmentation pattern of M7A is shown in Figure S5(D). Some of the product ions of M7A are the same with M7B, however there are unique diagnostic product ions that allowed us to identify the position of hydroxylation (M7A⁴, M7A⁶, M7A¹¹, M7A¹⁴). The MS/MS of [M7A + H]⁺ (Figure S10(C,D)) revealed a product ion (M7A¹) at *m/z* 454.28 characterized by the loss of water (-H₂O, 18 Da) indicating that the precursor ion is indeed formed as a result of P450 hydroxylation of the parent compound. The loss of water to produce M7A¹ is followed by subsequent loss of hydrogen fluoride to produce M7A³ at *m/z* 434.35. A unique diagnostic product ion of M7A is the neutral loss of hydroxyindene to product ion M7A⁴ with *m/z* 340.31 which is an indication that M7A is a metabolite formed as a result of hydroxylation of the indan moiety of ¹⁹F-[C₈-6-I]. This is consistent with hydroxylation of C₈-6-I where the indan moiety is also hydroxylated to M2 (see Figure 2(B)). M7A⁶ is a product ion which results from the loss of hydrogen fluoride from M7A⁴ followed by the loss of methyl isocyanate and 6-heptanenitrile to produce M7A¹¹ at *m/z* 263.36 and M7A¹³ at *m/z* 194.14 respectively. Overall, the first fragmentation pattern of [M7A + H]⁺ indicates that M7A is a monohydroxylated metabolite is as a result of hydroxylation on the indan of ¹⁹F-[C₈-6-I].

M7B shares some common product ions with M7A, however, there are unique product ions exclusive only to M7B (M7B², M7B⁵, M7B⁷, M7B¹⁰, M7B¹², M7B¹⁵). M7B⁵ with *m/z* 338.31 is characterized by sequential loss of water from [M7B + H]⁺ to produce M7B¹ at *m/z* 454.28 followed by loss of indene (Figure S10(E)). The loss of indene instead of hydroxyindene suggests that water loss is from the caffeine moiety of ¹⁹F-[C₈-6-I]. M7B⁵ further dissociates into M7B⁸ at *m/z* 321.24 by loss of ammonia (-NH₃, 17 Da) and M7B¹⁰ at *m/z* 301.64 by further loss of hydrogen fluoride (-HF, 20 Da) to produce a stable terminal alkyne. Also, the loss of hydrogen fluoride, indene and water produces a unique diagnostic product ion (M7B⁷) at *m/z* 318.28 having a terminal alkyne.

The formation of a stable terminal alkyne instead of alkene is an indication that the alkyl fluoride of caffeine is hydroxylated. Thus, M7B is a mono-hydroxylated metabolite from hydroxylation of the alkyl fluoride linker of ^{19}F -[C₈-6-I]. M7B⁷ can further fragment to M7B¹² at m/z 261.21 by loss of methyl isocyanate. The unique formation of a terminal alkyne from M7B fragmentation is diagnostic for the M7B metabolite. This alkyne formation is only possible as a result of loss of water and hydrogen fluoride at the terminal alkyl fluoride linker on the caffeine moiety. We do not know for sure if hydroxylation occurred on carbon 1 (C₁) or carbon 2 (C₂), but since we do not observe either defluorination or carbonylation metabolic pathways, we believe that the hydroxyl group is most likely one carbon away from the terminal fluoromethyl group at carbon-2.

Metabolites M8A and M8B possess the same retention time and are both 14 Da less than the parent compound. This is consistent with the non-fluorinated C₈-6-I in which M5A and M5B correspond to N1 and N3 demethylation (see Figure 5(C,D)). The MS/MS spectrum of the precursor ion (m/z 442.27) reveals three major diagnostic peaks: (M8A¹) at m/z 326.26 corresponding to the loss of indene from the precursor ion, (M8A²) at m/z 306.37 corresponding to the loss of indene followed by loss of hydrogen fluoride and, (M8A³) at m/z 309.35 corresponding to the loss of indene followed by loss of terminal ammonia. Product ion M8A⁴ at m/z 295.33 is produced as a result of methyl amine loss from M8A¹ and this product ion can further lose hydrogen fluoride to yield M8A⁶ (Figure S11(A,B)). Two product ions allowed us to determine that there are two demethylated metabolites and the position of demethylation. The first product ion is the loss of isocyanic acid (O=C=NH, 43 Da) from M8A² at m/z 306.37 to M8A⁷ at m/z 263.36. The loss of isocyanic acid instead of methyl isocyanate indicates that N1 of the precursor ion lacks a methyl group (Figure S11(B)). Conversely, product ion M8B⁸ with m/z 249.36 corresponds to the loss of methyl isocyanate (O=C=NCH₃, 57 Da) from M8B² (Figure S11(C)). This indicates that the N1 of the precursor ion has a methyl group present, however the loss of 14 Da is as a result of the lack of methyl group on N3. Therefore, M8A and M8B are both N1 and N3 demethylated metabolites of the caffeine moiety of ^{19}F -[C₈-6-I].

Metabolism of ^{19}F -[C₈-6-C₈]

Metabolism of ^{19}F -[C₈-6-C₈] revealed one major metabolite, M9 (Figure S12(B)). The m/z of M9 is 533.20 which is 16 Da higher than the m/z of ^{19}F -[C₈-6-C₈] which suggests M9 is a hydroxylated metabolite. MS/MS analysis of [M9 + H]⁺ revealed a major diagnostic product ion (M9³) at m/z 495.28 which corresponds to the loss of water and hydrogen fluoride confirming that the precursor ion is indeed a hydroxylated metabolite. The fragmentation pattern which leads to a stable terminal propyl alkyne on the caffeine moiety by loss of water and hydrogen fluoride for M9³ suggests that the hydroxylation of ^{19}F -[C₈-6-C₈] is almost certainly on the alkyl fluoride linker (Figure S12(A,B)). Similar to ^{19}F -[C₈-6-I], we do not observe any defluorination or carbonylation for ^{19}F -[C₈-6-C₈] which leads us to conclude that the hydroxylation is

most likely one carbon away from the fluoromethyl on carbon-2. The complete fragmentation pattern of M9 follows that observed for C₈-6-C₈ and ^{19}F -[C₈-6-C₈] (Figure S12(B)).

Metabolism of ^{19}F -[C₈-6-N]

The M10 metabolite of ^{19}F -[C₈-6-N] (Figure S13(A,B)) has a similar fragmentation pathway as the M6 metabolite of ^{19}F -[C₈-6-I]. The molecular formula and exact mass of M6 and M10 are the same indicating they both have the same molecular structure suggesting that M10 corresponds to two *N*-dealkylations of ^{19}F -[C₈-6-N] at the nicotine moiety, leaving a terminal aminoalkyl linker.

M11 is 16 Da higher than the parent compound ^{19}F -[C₈-6-N] indicating hydroxylation and we sought to confirm whether this had occurred on the alkyl fluoride linker. Unlike ^{19}F -[C₈-6-I] and ^{19}F -[C₈-6-C₈] which indicated hydroxylation of the alkyl fluoride, our fragmentation data for ^{19}F -[C₈-6-N] metabolite M11 is not consistent with this observation. The MS/MS spectrum of M11 (Figure S13(C)) shows an abundant diagnostic product ion at m/z 469.30 (M11¹) originating from the neutral loss of a water molecule from the precursor ion at m/z 487.35 [M11 + H]⁺ (Figure S13(D)). A second diagnostic product ion at m/z 467.46 (M11²) corresponds to the neutral loss of hydrogen fluoride (20 Da) from the precursor ion [M11 + H]⁺ confirming M11 as a metabolite of ^{19}F -[C₈-6-N], however the additional 16 Da compared to loss of HF from ^{19}F -[C₈-6-N] (Figure S6(B)) confirms hydroxylation does not occur on the alkyl fluoride. M11³ with m/z 449.45 is a result of both the loss of water (20 Da) and hydrogen fluoride (20 Da) from [M11 + H]⁺. The diagnostic product ion (M11⁴) at m/z 323.31 results from neutral loss of hydroxy nornicotine (C₉H₁₂N₂O₂, 164 Da) from [M11 + H]⁺. Similar to C₈-6-N, the diagnostic neutral loss of hydroxy nornicotine (C₉H₁₂N₂O₂, 164 Da) suggests that the hydroxyl group is located on the nicotine moiety of M11. M11¹⁰ at m/z 148.14 corresponds to the loss of hydrogen fluoride (-HF, 20 Da) and C₁₆H₂₅N₅O₂ (319 Da) from [M11 + H]⁺. Together, the product ions M11² at m/z 467.46, M11⁴ at m/z 323.31 and M11¹⁰ at m/z 148.17 strongly support hydroxylation of ^{19}F -[C₈-6-N] taking place on the nicotine portion of the compound.

Other product ions such as M11⁵ with m/z 303.34, M11⁶ with m/z 301.25, M11⁷ with m/z 263.26, M11⁸ with m/z 194.14 and M11¹² with m/z 106.01 are consistent with the tandem mass spectrometry fingerprint of ^{19}F -[C₈-6-N] (Figure S6). The absence of a stable terminal alkyne in the fragmentation pattern of [M11 + H]⁺ together with the fragment ions described support hydroxylation occurring on the nicotine and is consistent with a lack of hydroxylation on the alkyl fluoride linker.

Caffeine N7-linked propyl fluoro PET imaging probes

Five metabolic pathways were observed in HLM, MLM and RLM for ^{19}F -[C₈-6-I] (dealkylation (M6), aminoindan hydroxylation (M7A), N7-propyl fluoride hydroxylation (M7B), N1-demethylation (M8A), N3-demethylation (M8B) Figure 7(A));

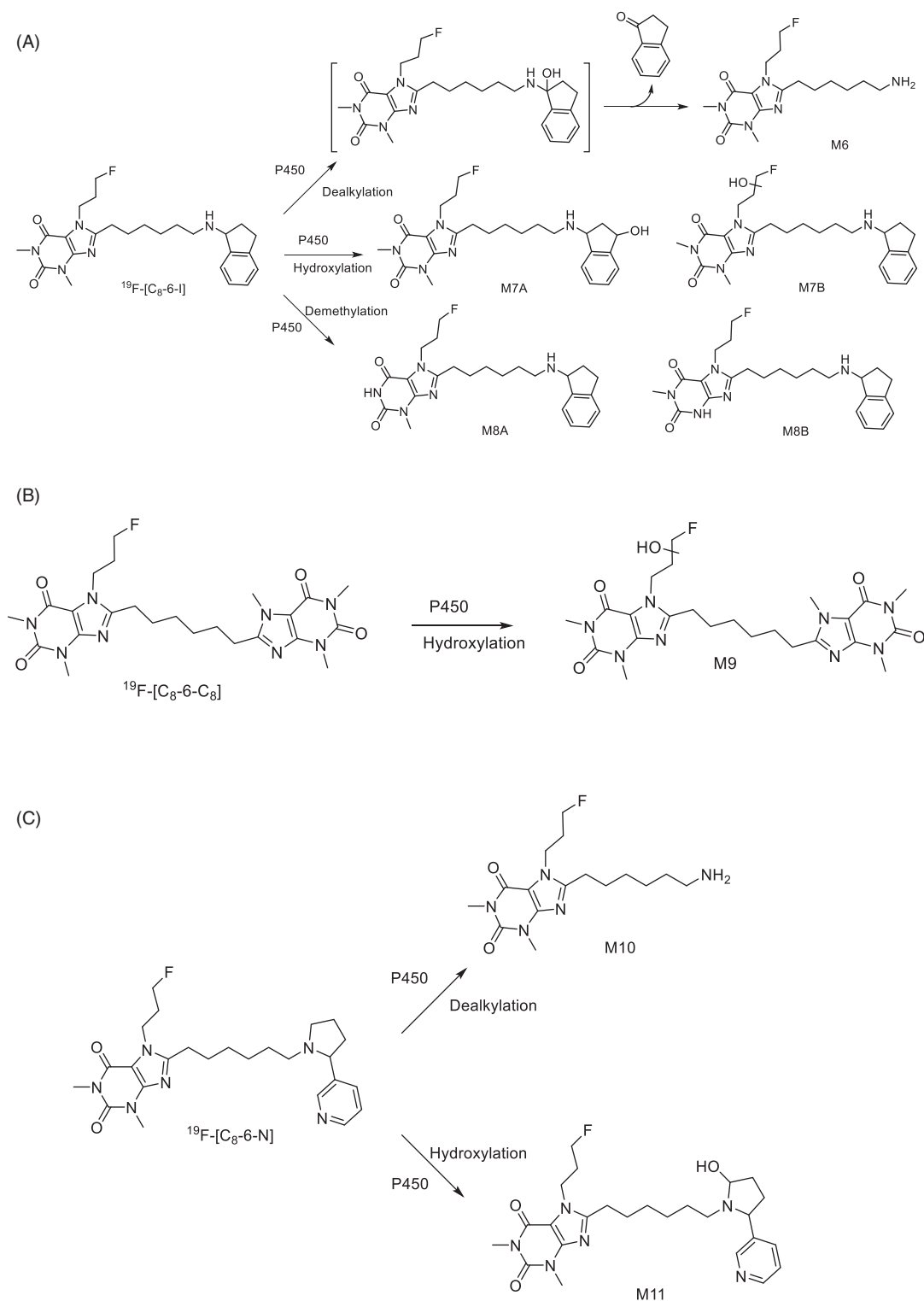


Figure 7. The proposed metabolic pathway for ^{19}F -[C₈-6-I] (A), ^{19}F -[C₈-6-C₈] (B) and ^{19}F -[C₈-6-N] (C) in human, mouse, and rat liver microsomes.

one metabolic pathway was observed for ^{19}F -[C₈-6-C₈] (N7-propyl fluoride hydroxylation (M9) **Figure 7(B)**) and two metabolic pathways were found for ^{19}F -[C₈-6-N] (dealkylation (M10) and nicotine hydroxylation (M11) **Figure 7(C)**). In addition, no N7-propyl fluoride hydroxylation was observed for ^{19}F -[C₈-6-N]. More critically, no *in vitro* defluorination, carbonylation or N7 dealkylation was observed for any of our

fluorinated bifunctional compounds in either HLM, RLM or MLM. We believe this supports our decision to incorporate the ^{18}F radioisotope at the N7 position on the caffeine scaffold of these bifunctional compounds.

Apart from the potential use of ^{18}F -labelled compounds for PET imaging, fluorine substitution is commonly employed in drug development due to its physical properties such as

strong carbon fluorine bond (C-F energy bond of 112 kcal/mol) as compared to carbon-hydrogen bond (C-H energy bond of 98 kcal/mol) and small van der Waals radius (1.47 Å) (Jacobson et al. 2015). However, it is important to develop fluorine labelled compounds that do not undergo defluorination *in vivo* as some fluorinated drugs in the past have been found to undergo metabolism to toxicologically relevant species such as methoxyflurane, widely used as an anaesthesia in the 1960s, which was found to be associated with nephrotoxicity due to extensive metabolism of methoxyflurane and high serum concentrations of inorganic fluoride (Park and Kitteringham 1994). Moreover, rapid defluorination of ^{18}F -labelled compounds makes interpretation of PET images ambiguous due to rapid accumulation of fluoride ion in bones and skull (Bonomi et al. 2018). Our *in vitro* metabolism studies indicate that we do not observe metabolic defluorination allowing us to further investigate our ^{18}F analogues for *in vivo* distribution. It should be noted however, that we will need to interpret our PET results carefully as de-fluorination may occur via other mechanisms than those restricted to hepatic microsomes, and metabolic N-dealkylation products will result in fluorine containing metabolites.

Conclusion

In this study, we evaluated the metabolic stability of C₈-6-N, C₈-6-I, C₈-6-C₈, ^{19}F -[C₈-6-I], ^{19}F -[C₈-6-C₈] and ^{19}F -[C₈-6-N] in HLM, MLM, and RLM. Accurate mass measurement and tandem mass spectrometry were used to identify and elucidate the structure of the corresponding metabolites of the bifunctional compounds in HLM, MLM, and RLM. The caffeine moiety of the tested compounds C₈-6-N, C₈-6-C₈, ^{19}F -[C₈-6-N] and ^{19}F -[C₈-6-C₈] was stable to *in vitro* Phase 1 metabolism, whereas the nicotine and aminoindan moieties underwent hydroxylation, presumably as a result of cytochrome P450 mediated metabolism. The caffeine moiety of C₈-6-I and ^{19}F -[C₈-6-I] underwent N3 and N1 demethylation similar to N3 and N1 demethylation of caffeine to paraxanthine and theobromine. Hydroxylation of the alkyl fluoride moiety was observed for ^{19}F -[C₈-6-C₈] and ^{19}F -[C₈-6-I] but not for ^{19}F -[C₈-6-N] and since [C₈-6-N] was observed to be extensively metabolized, this suggests a greater metabolic susceptibility of the nicotine than the alkyl fluoride linker. Whether this could affect the use of ^{19}F -[C₈-6-N] in our PET studies remains to be seen. No defluorinated metabolites were observed for any of our ^{19}F -bifunctional compounds indicating that the fluorination of the caffeine moiety with propyl fluoride is suitable for the synthesis of ^{18}F -bifunctional compounds for PET imaging and evaluation of biodistribution in animal studies. Finally, the same metabolites were observed for all compounds in HLM, MLM, and RLM, suggesting that mouse and rat may be useful surrogates for future animal studies of these bifunctional compounds.

Disclosure statement

No potential conflict of interest was reported by the author(s)

Funding

This work was supported by Natural Sciences and Engineering Research Council of Canada; Sylvia Fedoruk Canadian Centre for Nuclear Innovation; College of Pharmacy and Nutrition Graduate Scholarship; Department of Chemistry Graduate Scholarship.

References

- Agundez JA, Garcia-Martin E, Alonso-Navarro H, Jimenez-Jimenez FJ. 2013. Anti-Parkinson's disease drugs and pharmacogenetic considerations. *Expert Opin Drug Metab Toxicol.* 9 (7):859–874.
- Bar Am O, Amit T, Youdim MB. 2004. Contrasting neuroprotective and neurotoxic actions of respective metabolites of anti-Parkinson drugs rasagiline and selegiline. *Neurosci Lett.* 355 (3):169–172.
- Bar-Am O, Weinreb O, Amit T, Youdim MB. 2010. The neuroprotective mechanism of 1-(R)-aminoindan, the major metabolite of the anti-parkinsonian drug rasagiline. *J Neurochem.* 112 (5):1131–1137.
- Barreto GE, larkov A, Moran VE. 2014. Beneficial effects of nicotine, cotinine and its metabolites as potential agents for Parkinson's disease. *Front Aging Neurosci.* 6:340.
- Benowitz NL, Hukkanen J, and Jacob P. 3rd, 2009. Nicotine chemistry, metabolism, kinetics and biomarkers. *Handb Exp Pharmacol.* 192: 29–60.
- Berthou F, Ratanasavanh D, Alix D, Carlhant D, Riche C, Guillouzo A. 1988. Caffeine and theophylline metabolism in newborn and adult human hepatocytes; comparison with adult rat hepatocytes. *Biochem Pharmacol.* 37(19):3691–3700.
- Berthou F, Ratanasavanh D, Riche C, Picart D, Voirin T, Guillouzo A. 1989. Comparison of caffeine metabolism by slices, microsomes and hepatocyte cultures from adult human liver. *Xenobiotica.* 19(4):401–417.
- Bianco G, Abate S, Labella C, Cataldi TR. 2009. Identification and fragmentation pathways of caffeine metabolites in urine samples via liquid chromatography with positive electrospray ionization coupled to a hybrid quadrupole linear ion trap(LTQ) and Fourier transform ion cyclotron resonance mass spectrometry and tandem mass spectrometry. *Rapid Commun Mass Spectrom.* 23 (7):1065–1074.
- Bier D, Hartmann R, Holschbach M. 2013. Collision-induced dissociation studies of caffeine in positive electrospray ionisation mass spectrometry using six deuterated isotopomers and one N1-ethylated homologue. *Rapid Commun Mass Spectrom.* 27(8):885–895.
- Bonomi RE, Laws M, Popov V, Kamal S, Potukutchi S, Shavrin A, Lu X, Turkman N, Liu RS, Mangner T, et al. 2018. A Novel Substrate Radiotracer for Molecular Imaging of SIRT2 Expression and Activity with Positron Emission Tomography. *Mol Imaging Biol.* 20(4):594–604.
- Brandange S, Lindblom L. 1979. Enzyme Aldehyde Oxidase Is an Iminium Oxidase - Reaction with Nicotine Delta-1'(5')Iminium Ion. *Biochem Biophys Res Commun.* 91(3):991–996.
- Campbell ME, Grant DM, Inaba T, Kalow W. 1987. Biotransformation of caffeine, paraxanthine, theophylline, and theobromine by polycyclic aromatic hydrocarbon-inducible cytochrome(s) P-450 in human liver microsomes. *Drug Metab Dispos.* 15(2):237–249.
- Chau KY, Cooper JM, Schapira AH. 2010. Rasagiline protects against alpha-synuclein induced sensitivity to oxidative stress in dopaminergic cells. *Neurochem Int.* 57(5):525–529.
- Chen K, Chen X. 2010. Design and development of molecular imaging probes. *Curr Top Med Chem.* 10(12):1227–1236.
- Chênevert R, Mohammadi-Ziarani G, Caron D, Dasser M. 1999. Chemoenzymatic enantioselective synthesis of (-)-enterolactone. *Can J Chem.* 77(2):223–226.
- Davie CA. 2008. A review of Parkinson's disease. *Br Med Bull.* 86: 109–127.
- de Biase S, Merlino G, Lorenzut S, Valente M, Gigli GL. 2014. ADMET considerations when prescribing novel therapeutics to treat restless legs syndrome. *Expert Opin Drug Metab Toxicol.* 10(10):1365–1380.
- Deffereos SN, Dodou E, Andronis C, Persidis A. 2012. From depression to neurodegeneration and heart failure: re-examining the potential of MAO inhibitors. *Expert Rev Clin Pharmacol.* 5(4):413–425.

- Dimpfel W, Hoffmann JA. 2011. Effects of rasagiline, its metabolite aminoindan and selegiline on glutamate receptor mediated signalling in the rat hippocampus slice in vitro. *BMC Pharmacol.* 11:2.
- Ferrero JL, Neims AH. 1983. Metabolism of caffeine by mouse liver microsomes: GSH or cytosol causes a shift in products from 1,3,7-trimethylurate to a substituted diaminouracil. *Life Sci.* 33(12):1173–1178.
- Forno LS. 1996. Neuropathology of Parkinson's disease. *J Neuropathol Exp Neurol.* 55(3):259–272.
- Grant DM, Campbell ME, Tang BK, Kalow W. 1987. Biotransformation of caffeine by microsomes from human liver. Kinetics and inhibition studies. *Biochem Pharmacol.* 36(8):1251–1260.
- Hecht SS, Hochalter JB, Villalta PW, Murphy SE. 2000. 2'-Hydroxylation of nicotine by cytochrome P450 2A6 and human liver microsomes: formation of a lung carcinogen precursor. *Proc Natl Acad Sci U S A.* 97(23):12493–12497.
- Hughes AJ, Ben-Shlomo Y, Daniel SE, Lees AJ. 1992. What features improve the accuracy of clinical diagnosis in Parkinson's disease: a clinicopathologic study. *Neurology.* 42(6):1142–1146.
- Hughes AJ, Daniel SE, Lees AJ. 2001. Improved accuracy of clinical diagnosis of Lewy body Parkinson's disease. *Neurology.* 57(8):1497–1499.
- Jacobson O, Kiesewetter DO, Chen X. 2015. Fluorine-18 radiochemistry, labeling strategies and synthetic routes. *Bioconjug Chem.* 26(1):1–18.
- Jia L, Liu X. 2007. The conduct of drug metabolism studies considered good practice (II): in vitro experiments. *Curr Drug Metab.* 8(8): 822–829.
- Kakish J, Allen KJ, Harkness TA, Krol ES, Lee JS. 2016. Novel Dimer Compounds That Bind α -Synuclein Can Rescue Cell Growth in a Yeast Model Overexpressing α -Synuclein. A Possible Prevention Strategy for Parkinson's Disease. *ACS Chem Neurosci.* 7(12):1671–1680.
- Kakish J, Lee D, Lee JS. 2015. Drugs That Bind to α -Synuclein: Neuroprotective or Neurotoxic? *ACS Chem Neurosci.* 6(12):1930–1940.
- Litvan I, MacIntyre A, Goetz CG, Wenning GK, Jellinger K, Verny M, Bartko JJ, Jankovic J, McKee A, Brandel JP, et al. 1998. Accuracy of the clinical diagnoses of Lewy body disease, Parkinson disease, and dementia with Lewy bodies: a clinicopathologic study. *Arch Neurol.* 55(7):969–978.
- Medana C, Santoro V, Dal Bello F, Sala C, Pazzi M, Sarro M, Calza P. 2016. Mass spectrometric fragmentation and photocatalytic transformation of nicotine and cotinine. *Rapid Commun Mass Spectrom.* 30(24): 2617–2627.
- Mendes VM, Coelho M, Tome AR, Cunha RA, Manadas B. 2019. Validation of an LC-MS/MS Method for the Quantification of Caffeine and Theobromine Using Non-Matched Matrix Calibration Curve. *Molecules.* 24(16):2863.
- Mukai M, Uchimura T, Zhang X, Greene D, Vergeire M, Cantillon M. 2018. Effects of Rifampin on the Pharmacokinetics of a Single Dose of Istradefylline in Healthy Subjects. *J Clin Pharmacol.* 58(2):193–201.
- Murphy PJ. 1973. Enzymatic oxidation of nicotine to nicotine 1'(5') iminium ion. A newly discovered intermediate in the metabolism of nicotine. *J Biol Chem.* 248(8):2796–2800.
- Nwabufu CK, El-Anead A, Krol ES. 2019. Tandem mass spectrometric analysis of novel caffeine scaffold-based bifunctional compounds for Parkinson's disease. *Rapid Commun Mass Spectrom.* 33(23): 1792–1803.
- Park BK, Kitteringham NR. 1994. Effects of fluorine substitution on drug metabolism: pharmacological and toxicological implications. *Drug Metab Rev.* 26(3):605–643.
- Patil SP, Jain PD, Ghumatkar PJ, Tambe R, Sathaye S. 2014. Neuroprotective effect of metformin in MPTP-induced Parkinson's disease in mice. *Neuroscience.* 277:747–754.
- Peterson LA, Trevor A, Castagnoli N. Jr., 1987. Stereochemical studies on the cytochrome P-450 catalyzed oxidation of (S)-nicotine to the (S)-nicotine delta 1'(5')-iminium species. *J Med Chem.* 30(2):249–254.
- Postuma RB, Lang AE, Munhoz RP, Charland K, Pelletier A, Moscovich M, Filla L, Zanatta D, Rios Romanets S, Altman R, et al. 2012. Caffeine for treatment of Parkinson disease: a randomized controlled trial. *Neurology.* 79(7):651–658.
- Prediger RD. 2010. Effects of caffeine in Parkinson's disease: from neuroprotection to the management of motor and non-motor symptoms. *J Alzheimers Dis.* 20 Suppl 1(Suppl 1):S205–S220.
- Quik M. 2004. Smoking, nicotine and Parkinson's disease. *Trends Neurosci.* 27(9):561–568.
- Quik M, Perez XA, Bordia T. 2012. Nicotine as a potential neuroprotective agent for Parkinson's disease. *Mov Disord.* 27(8):947–957.
- Rajput AH, Rozdilsky B, Rajput A. 1991. Accuracy of clinical diagnosis in parkinsonism—a prospective study. *Can J Neurol Sci.* 18(3):275–278.
- Rizzo G, Copetti M, Arcuti S, Martino D, Fontana A, Logroscino G. 2016. Accuracy of clinical diagnosis of Parkinson disease: A systematic review and meta-analysis. *Neurology.* 86(6):566–576.
- Ross GW, Petrovitch H. 2001. Current evidence for neuroprotective effects of nicotine and caffeine against Parkinson's disease. *Drugs Aging.* 18(11):797–806.
- Samii A, Nutt JG, Ransom BR. 2004. Parkinson's disease. *Lancet.* 363(9423):1783–1793.
- Schrag A, Ben-Shlomo Y, Quinn N. 2002. How valid is the clinical diagnosis of Parkinson's disease in the community? *J Neurol Neurosurg Psychiatry.* 73(5):529–534.
- Sterling J, Veinberg A, Lerner D, Goldenberg W, Levy R, Youdim M, Finberg J. 1998. N-propargyl-1-aminoindan (rasagiline) and derivatives: highly selective and potent inhibitors of monoamine oxidase B. *Journal of Neural Transmission. Supplementa.* 52:301–305.
- Temporal KH, Scott KS, Mohr ALA, Logan BK. 2017. Metabolic Profile Determination of NBOMe Compounds Using Human Liver Microsomes and Comparison with Findings in Authentic Human Blood and Urine. *J Anal Toxicol.* 41(7):646–657.
- Tolosa E, Gaig C, Santamaria J, Compta Y. 2009. Diagnosis and the pre-motor phase of Parkinson disease. *Neurology.* 72(7 Suppl):S12–S20.
- Uversky VN. 2008. Alpha-synuclein misfolding and neurodegenerative diseases. *Curr Protein Pept Sci.* 9(5):507–540.
- Wahlqvist ML, Lee MS, Hsu CC, Chuang SY, Lee JT, Tsai HN. 2012. Metformin-inclusive sulfonylurea therapy reduces the risk of Parkinson's disease occurring with Type 2 diabetes in a Taiwanese population cohort. *Parkinsonism Relat Disord.* 18(6):753–758.
- Wang T, Yang L, Hua J, Xie H, Jiang X, Wang L. 2016. Simultaneous bioanalysis of rasagiline and its major metabolites in human plasma by LC-MS/MS: Application to a clinical pharmacokinetic study. *J Pharm Biomed Anal.* 125:280–285.